energies

MDPI

Article

Fluorine-Doped $LiNi_{0.8}Mn_{0.1}Co_{0.1}O_2$ Cathode for High-Performance Lithium-Ion Batteries

Hyeona Kim, Sung-Beom Kim, Deok-Hye Park and Kyung-Won Park *

Department of Chemical Engineering, Soongsil University, Seoul 06987, Korea; cessp2000@naver.com (H.K.); k3331247@nate.com (S.-B.K.); dehui.piao@gmail.com (D.-H.P.)

* Correspondence: kwpark@ssu.ac.kr; Tel.: +82-2-820-0613; Fax: +82-2-812-5378

Received: 20 August 2020; Accepted: 10 September 2020; Published: 14 September 2020

Abstract: For advanced lithium-ion batteries, $LiNi_xCo_yMn_zO_2$ (x + y + z = 1) (NCM) cathode materials containing a high nickel content have been attractive because of their high capacity. However, to solve severe problems such as cation mixing, oxygen evolution, and transition metal dissolution in $LiNi_{0.8}Co_{0.1}Mn_{0.1}O_2$ cathodes, in this study, F-doped $LiNi_{0.8}Co_{0.1}Mn_{0.1}O_2$ (NCMF) was synthesized by solid-state reaction of a NCM and ammonium fluoride, followed by heating process. From X-ray diffraction analysis and X-ray photoelectron spectroscopy, the oxygen in NCM can be replaced by F^- ions to produce the F-doped NCM structure. The substitution of oxygen with F^- ions may produce relatively strong bonds between the transition metal and F and increase the c lattice parameter of the structure. The NCMF cathode exhibits better electrochemical performance and stability in half- and full-cell tests compared to the NCM cathode.

Keywords: fluorine; doping; $LiNi_{0.8}Co_{0.1}Mn_{0.1}O_2$; cathode; lithium-ion batteries

1. Introduction

Since Li-ion batteries (LIBs) have been mainly utilized as the key power source in various applications, next-generation LIBs must exhibit high energy density, high power, high capacity, fast charging/discharging rate, and stability [1–4]. To satisfy these requirements, it is essential to identify inexpensive cathode materials with excellent capacity, volume, and performance [5]. $LiCoO_2$ (LCO), a representative cathode with a 3d layered structure, has critical limitations, such as the high cost of cobalt and a relatively low reversible capacity, which offset its advantages of superior cycling performance and excellent stability [6–8].

Ni-based layered cathode materials, i.e., $LiNi_xCo_yMn_zO_2$ (x + y + z = 1) (NCM), have received attention recently as a promising alternative to LCO [9]. Specifically, NCM materials with high nickel contents (high-Ni cathode) have been used owing to their higher capacity [10]. However, serious problems with high-Ni cathodes have been observed during charging and discharging, such as destruction of the layered structure, cation mixing, oxygen evolution, and transition metal dissolution; these phenomena promote the irreversible consumption of Li^+ ions and thus degrade the LIB performance [11–13]. Various methods, such as coating, composite structure formation, cation/anion doping, and structure control, have been extensively studied to address these limitations of high-Ni cathodes [14–18]. Furthermore, the battery management system is also important for the improvement of Li-ion battery [19–21]. In particular, anionic elements such as F, Cl, and S can be doped into the oxygen sites of layered cathode materials [22]. Anion doping may directly affect the anionic redox process and effectively enhance the electrochemical performance, preventing cation mixing, oxygen evolution, and structural collapse [23]. Among these anionic dopants, F can prevent damage to the cathode by the generation of Hydrogen Fluoride (HF) through the dissociation of the electrolyte and the loss of oxygen in the lattice [24,25]. In this study, F-doped $LiNi_{0.8}Co_{0.1}Mn_{0.1}O_2$ (NCMF) was

synthesized by a solid-state reaction of a prepared precursor and ammonium fluoride, followed by heating. However, to compensate for a key disadvantage, i.e., uneven mixing of raw materials, the NCM precursor was prepared using a solvothermal synthesis [26]. The electrochemical performance and stability of the NCMF cathode were compared with those of an undoped $LiNi_{0.8}Co_{0.1}Mn_{0.1}O_2$ (NCM) cathode in half- and full-cell tests using $Li_4Ti_5O_{12}$ (LTO) as an anode.

2. Materials and Methods

2.1. Synthesis of NCM and NCMF

To prepare the NCM precursor with a target ratio of Ni/Co/Mn = 8:1:1, nickel acetate tetrahydrate (≥99.0%, Sigma Aldrich, Saint Louis, MO, USA), cobalt acetate tetrahydrate (≥98.0%, Sigma Aldrich), and manganese acetate tetrahydrate (≥99.0%, Sigma Aldrich) were dissolved in 50 mL of absolute ethanol (99.9%, Fisher scientific Korea Ltd., Seoul, Korea) in a Teflon-lined autoclave. The metal-salt mixture was then heated in a box furnace at 200 °C for 12 h. The heated sample was washed using centrifugation and dried in a 50 °C vacuum oven overnight. The NCM cathode was obtained by heating the precursor with lithium hydroxide monohydrate (≥99.0%, Sigma Aldrich) in an air atmosphere. Two-step heating was performed at 480 °C for 8 h and 720 °C for 12 h. In addition, NCMF (0.055 mol) was prepared by heating the as-prepared NCM with ammonium fluoride (≥98.0%, Sigma Aldrich) in air at 450 °C for 12 h.

2.2. Material Characterization

To confirm the crystal structure of the samples, an X-ray diffractometer (Bruker, Billerica, MA, USA, D2 Phase system) was operated at 40 kV and 100 mA with a Cu K_α X-ray source (λ = 0.15418 nm). The morphology and elemental distribution of the samples were observed by field-emission scanning electron spectroscopy (FE-SEM, Zeiss, Oberkochen, Germany, Gemini 300) at 15 kV and 100 mA with an X-ray source and by energy dispersive spectroscopy (EDS, Zeiss, Gemini 300). To characterize the chemical states of the samples, X-ray photoelectron spectroscopy (XPS, K-alpha, Thermo VG, Al K_α line: 1486.6 eV) was performed.

2.3. Cell Assembly and Electrochemical Characterization

The active cathode material (80 wt.%), Ketjen black (Wellcos, 10 wt.%), and polyvinylidene fluoride (PVDF, 10 wt.%, Alfa Aesar, Ward Hill, MA, USA, 20 wt.%) were mixed using a paste mixer. The prepared slurry was coated on a Cu foil by a doctor blade method to form the electrode. The coated electrode was dried in a 110 °C oven overnight. The electrolyte was prepared by adding 1.1 M $LiPF_6$ in EC: DEC = 1:1 to ethylene carbonate/diethyl carbonate. To characterize the electrochemical properties of the sample as a cathode for LIBs, a coin-type half-cell was assembled in an Ar-filled glove box using the electrode, electrolyte, polyethylene as a separator, and lithium metal as an anode. The charge/discharge behavior of the assembled cell was evaluated in a potential range of 2.8–4.3 V vs. Li/Li^+ using a multichannel battery tester (WBCS3000L, Wonatech Co., Seoul, Korea) at current densities of 20–400 mA g^{-1}. Cyclic voltammetry (CV) was performed in the potential range of 2.8–4.3 V vs. Li/Li^+ at a scan rate of 0.02 mV s^{-1}. Galvanostatic intermittent titration technique (GITT) measurements were carried out at the following conditions: 2.8–4.3 V vs. Li/Li^+, 20 mA g^{-1}, a pulse time = 10 min, a rest time = 60 min.

3. Results and Discussion

Figure 1a shows the wide-scan X-ray diffraction (XRD) patterns of the as-prepared NCM and NCMF samples. All the samples had a hexagonal layered structure (a-$NaFeO_2$, R-3m space group) with the main characteristic peaks corresponding to the (003), (006), (102), (104), (018), and (110) planes at 18.7°, 38°, 38.4°, 44.5°, 64.5°, and 65°, respectively [27–29]. The formation of a well-ordered, hexagonal, layered structure was demonstrated by the splitting of the (006)/(102) and (108)/(110) peaks and the

intensity ratio of >1.2 for the (003)/(104) [30]. However, in the NCMF, the replacement of oxygen with F^- ions can result in the partial reduction of the transition metal, increasing its ionic radius. Consequently, the c lattice parameter of the NCMF increased, as indicated by a larger d-spacing of the (003) plane and a low-angle peak shift (Figure 1b,c, Supplementary Materials Table S1) [31].

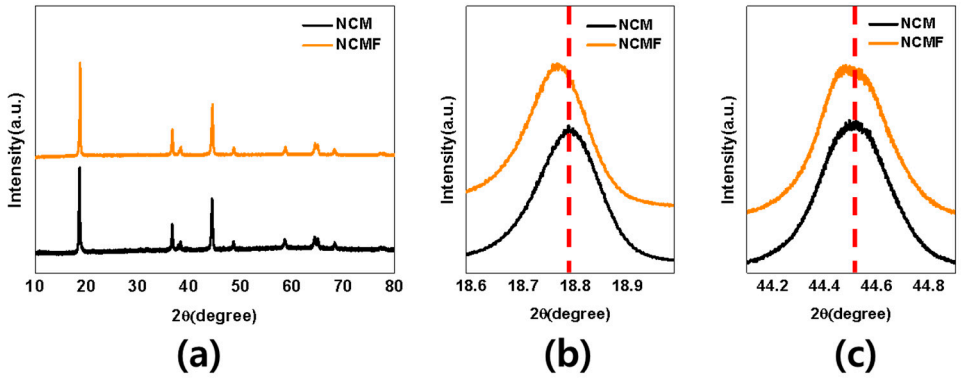

Figure 1. (**a**) Wide-angle XRD patterns and fine scans of (**b**) (003) and (**c**) (104) planes of NCM and NCMF.

The as-prepared NCM and NCMF samples showed irregular shapes and size distributions, as shown in Figure 2a,b, irrespective of the F doping. However, well-dispersed F was observed in the NCMF, indicating successful F doping. To investigate the replacement of oxygen with F^- ions at the oxygen sites, XPS analysis was performed (Figure 3 and Figure S1). In the O1s spectra, the characteristic peaks at 528–530 and 531–533 eV correspond to bonds between the transition metal (M) and oxygen and oxygen vacancies, respectively (Figure 3a–d). Compared with the NCM, the NCMF exhibited a lower area ratio of M–O bonds, indicating that it had fewer M–O bonds (Table S2) [32–35]. Furthermore, the Ni2p spectrum of NCMF consisted of characteristic peaks at 854–856 and 858–859 eV, which corresponded to Ni–O and M–F bonds, respectively (Figure 3b). By contrast, the NCM showed a characteristic peak at 854–856 eV, which corresponded to Ni–O bonds (Figure 3e). These results demonstrate that F^- ions replaced oxygen in the NCM, producing the F-doped NCM structure.

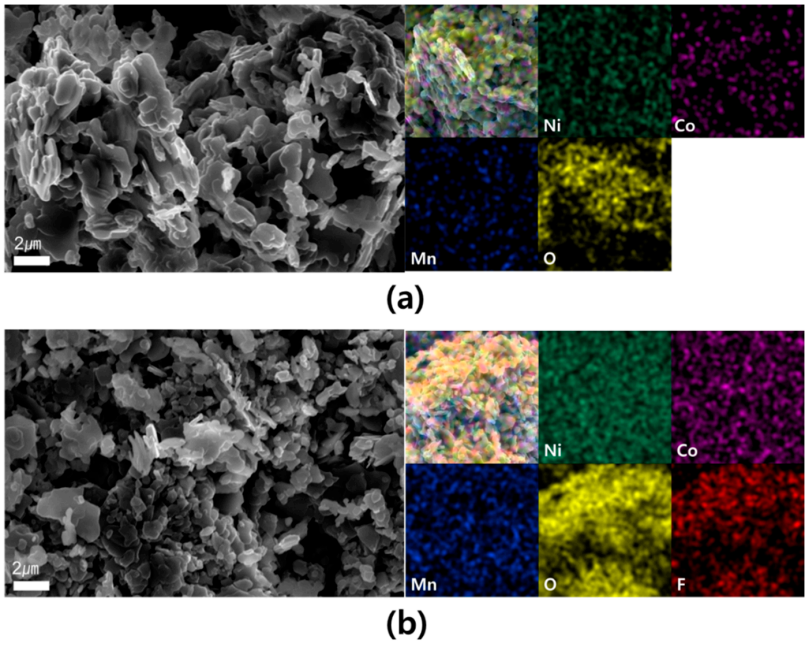

Figure 2. SEM and EDS mapping images of (**a**) NCM and (**b**) NCMF.

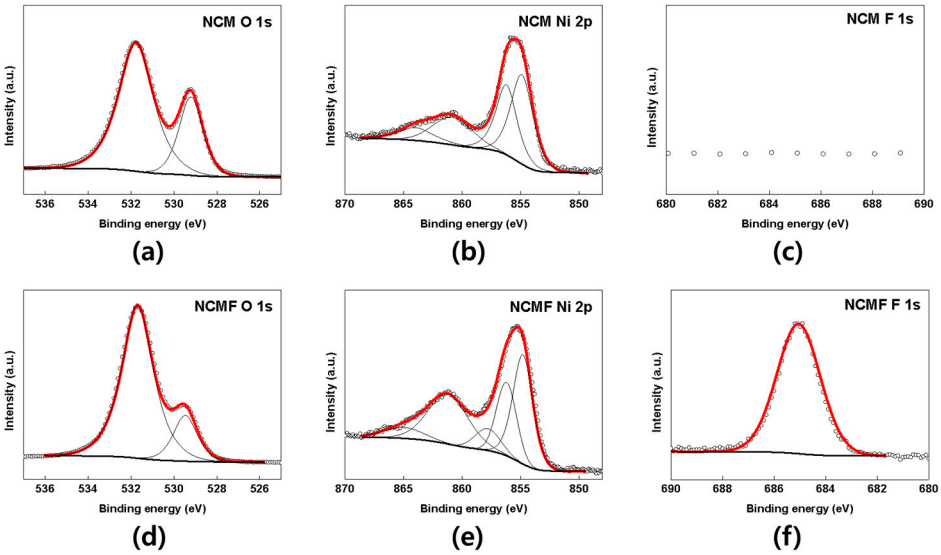

Figure 3. (**a**) O1s, (**b**) Ni2p, (**c**) F1s XPS spectra of NCM and (**d**) O1s, (**e**) Ni2p, (**f**) F1s XPS spectra of NCMF.

Figure 4a,b shows CVs of the NCM and NCMF cathodes at a scan rate of 0.02 mV s^{-1} in the potential range of 2.8–4.3 V vs. Li/Li^+. Three redox couple peaks corresponding to insertion/deinsertion reactions during charging/discharging were observed. In particular, during charging, the characteristic reversible peaks associated with the transitions, the hexagonal to monoclinic (H1–M), monoclinic to hexagonal (M–H2), and hexagonal to hexagonal phases (H2–H3), appeared at ~3.7, ~4.0, and ~4.2 V, respectively [36,37]. Figure 4c shows charge/discharge characteristic curves of the NCM and NCMF cathodes in the potential range of 2.8–4.3 V vs. Li/Li^+ at a current density of 40 mA g^{-1} for 150 cycles. The capacity retentions of the NCM and NCMF from the second to the 150th cycles were calculated to be 84% and 94%, respectively, from the ratios of discharge capacities. Charge/discharge curves of the NCM and NCMF cathodes were measured in the potential range of 2.8–4.3 V vs. Li/Li^+ at a current density of 100 mA g^{-1} for 100 cycles (Figure 4d and Figure S2). The capacity retentions of the NCM and NCMF at the second and 150th cycles were determined to be 58% and 93%, respectively, from the ratios of discharge capacities. The improved cycling performance of the NCMF cathode at both 40 and 100 mA g^{-1} compared to the NCM cathode may be attributed to the stable structure of NCMF, in which the bonds between the transition metal (M) and the fluorine dopant are more stable M–O bonds [38]. The increased d-spacing in NCMF, which was observed in the XRD results, may facilitate the insertion/deinsertion of Li^+ ions during cycling. Furthermore, the reduced interfacial resistance in NCMF can increase the mobility of Li^+ ions and, thus, significantly reduce the overpotential of NCMF during charging and discharging [39].

Figure 5a,b shows the charge/discharge curves of the NCM and NCMF cathodes measured at a current density of 40 mA g^{-1} in the potential range of 2.8–4.3 V vs. Li/Li^+ for 150 cycles. The variation of the discharge voltage, which is a key factor affecting the energy density, was 0.10 and 0.03 V between the second and 150th cycles for the NCM and NCMF, respectively (Figure 5d). Furthermore, as shown in Figure 5e, the energy density of the cells with NCM and NCMF cathodes were compared. The energy density retentions after 100 cycles, as a percentage of the energy density after two cycles, were 81% and 92% for the NCM and NCMF cathodes, respectively, indicating improved cycling stability of the NCMF cathode.

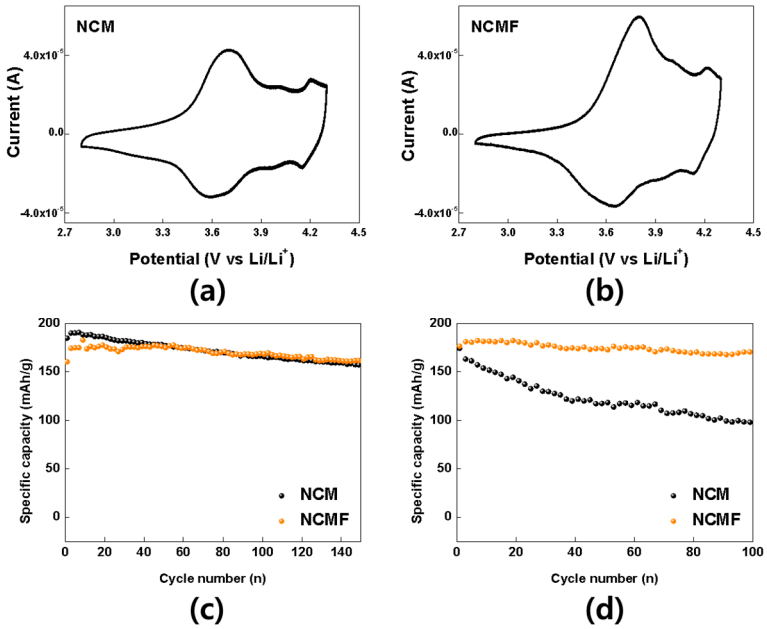

Figure 4. CVs of (**a**) NCM and (**b**) NCMF at a scan rate of 0.02 mV s^{-1} in the potential range of 0–2 V vs. Li/Li^+. Specific discharge capacities of the samples at a current density of (**c**) 40 mA g^{-1} and (**d**) 100 mA g^{-1} in the potential range of 2.8–4.3 V vs. Li/Li^+ for 150 cycles.

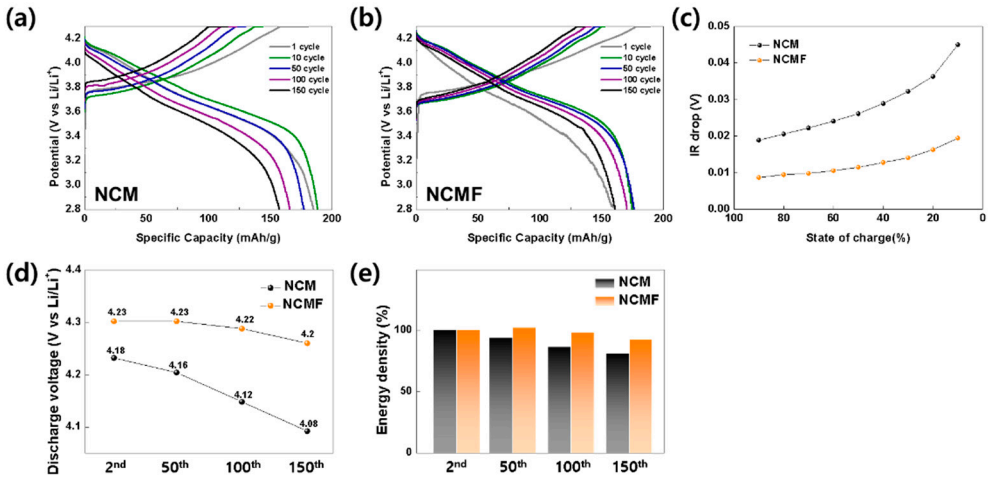

Figure 5. Charge/discharge curves of (**a**) NCM and (**b**) NCMF at a current density of 40 mA g^{-1} in the potential range of 2.8–4.3 V vs. Li/Li^+ for 150 cycles. (**c**) Plots of IR drop vs. charge state of the cathodes. Variations of (**d**) discharge voltages and (**e**) energy density between the second and 150th cycles for NCM and NCMF cathodes.

To determine the diffusion coefficient of Li^+ ions and the IR drop during cycling, GITT analysis was performed in the potential range of 2.8–4.3 V vs. Li/Li^+ at a current density of 20 mA g^{-1} with a pulse time of 10 min and a rest time of 60 min (Figure 5c and Figure S3). The diffusion coefficient of Li^+ ions can be calculated as follows [40]:

$$D_{Li^+} = \frac{4}{\pi\tau}\left(\frac{nV}{s}\right)^2\left(\frac{\Delta E_s}{\Delta E_t}\right)^2 \quad (1)$$

where τ is the time at a constant current, V is the volume of the electrode, s is the contact area between the electrode and electrolyte, ΔE_s is the variation of the equilibrium voltage, and ΔE_t is the voltage variation at the applied current. The Li^+ ion diffusion coefficients for the NCM and NCMF cathodes

were found to be 1.24×10^{-10} and 1.35×10^{-10} cm^2 s^{-1}, respectively. In addition, the IR drop of the NCMF cathode was 0.013 V, lower than that of the NCM cathode (0.028 V), indicating both reduced resistance to Li^+ ion diffusion and less variation of the discharge voltage. The enhanced Li^+ ion behavior into NCMF as an active material during cycling may be attributed to the F-doping of the cathode, which can increase the d-spacing of the NCM structure [41].

Figure 6a compares the cycling performance of the NCM and NCMF cathodes measured from 20 to 600 mA g^{-1}. The discharge capacities of the NCM and NCMF cathodes at different current densities were compared on the basis of the average capacity at a current density of 20 mA g^{-1} (Figure 6b). The NCMF cathode had a higher capacity in all the current density ranges than the NCM cathode. F-doping of the NCM can increase the d-spacing in the NCM structure, facilitating insertion and deinsertion of Li^+ ion during cycling. Furthermore, the relatively strong bonds between the transition metal and F in the F-doped cathode can enhance the structural stability and suppress phase transitions, i.e., the H2 to H3 and layered to rock-salt transitions, resulting in the superior cycling performance at high current densities [42,43].

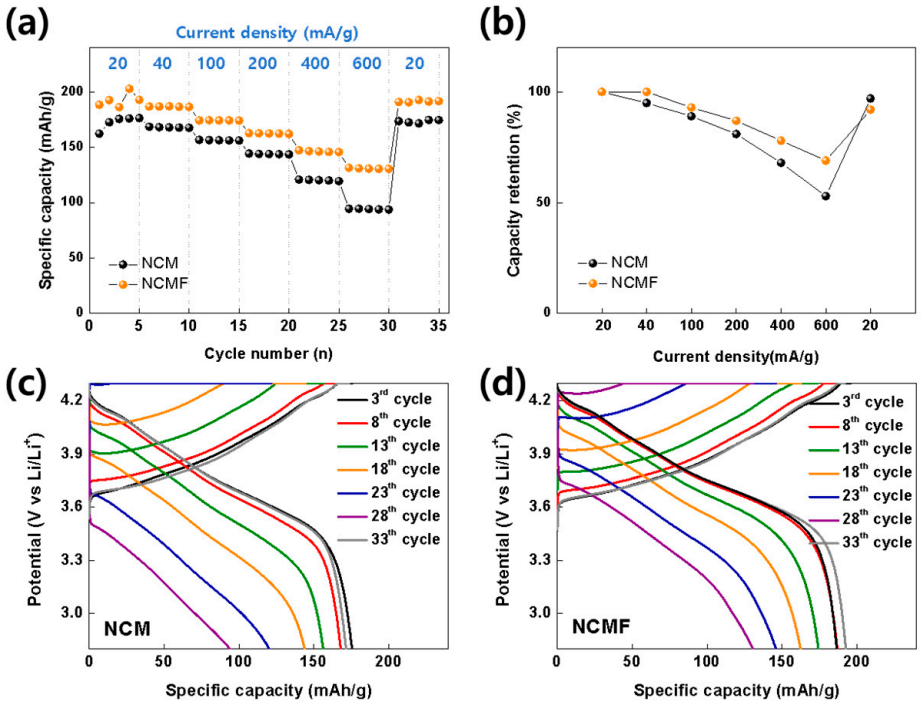

Figure 6. (**a**) Rate performance of cathode samples at various current densities ranging from 20 to 600 mA g^{-1} for five cycles each. (**b**) Capacity retention of the samples. Charge/discharge curves of (**c**) NCM and (**d**) NCMF cathodes at current densities ranging from 20 to 400 mA g^{-1}.

Figure 7a–d shows the cycling performance and charge/discharge curves of full cells consisting of the NCM and NCMF cathodes and $Li_4Ti_5O_{12}$ (LTO) as an anode (denoted as the NCM-LTO and NCMF-LTO, respectively) in the potential range of 0.3–3.2 V vs. Li/Li^+ at a current density of 100 mA g^{-1} for 50 cycles. The initial discharge capacities of the NCM-LTO and NCMF-LTO were 179 and 201 mAh g^{-1}, respectively. The energy densities of the NCM-LTO and NCMF-LTO in the first cycle were 337 and 412 Wh Kg^{-1}, respectively. The capacity retentions of the NCM-LTO and NCMF-LTO after 50 cycles were 63% and 88%, respectively. Thus, the cell with the NCMF cathode outperformed that with the NCM cathode, possibly owing to the enhanced structural stability and reduced resistance to Li^+ ion diffusion in the F-doped cathode.

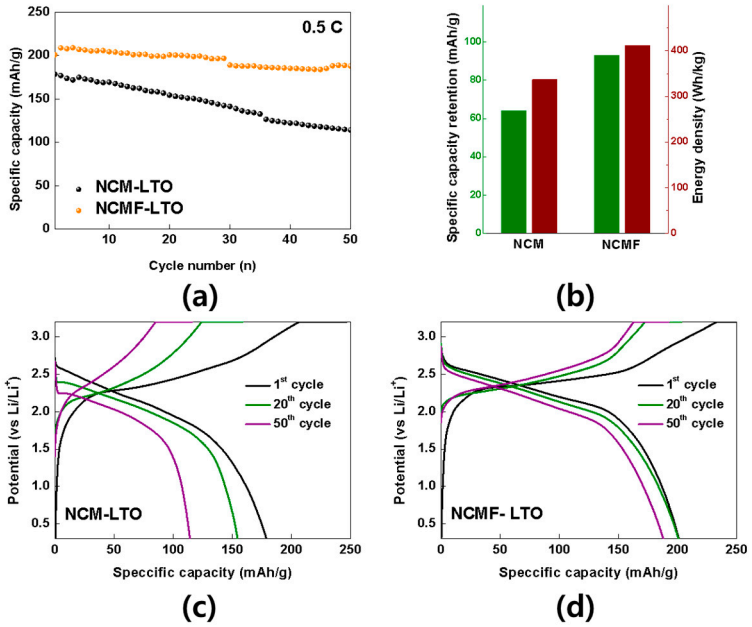

Figure 7. (**a**) Specific discharge capacities of the samples at a current density of 100 mA g^{-1} for 50 cycles. (**b**) Capacity retention and energy density of the samples. Charge-discharge curves of (**c**) NCM-LTO and (**d**) NCMF-LTO cells.

4. Conclusions

In summary, an NCMF cathode was synthesized by solid-state reaction with a prepared precursor and ammonium fluoride, followed by heating. The oxygen atoms in the NCM could be replaced with F^- ions, to produce a F-doped NCM structure. The substitution of F^- ions at the oxygen sites may produce relatively strong bonds between the transition metal and F and increase the c lattice parameter of the structure from 1.416 to 1.418 Å, enhancing the Li^+ ion diffusion coefficient in the NCMF cathode (1.24×10^{-10} to 1.35×10^{-10} cm^2 s^{-1}). Thus, the NCMF cathode exhibited the improved electrochemical performance (discharge capacity: 201 mAh g^{-1}, energy density: 412 Wh Kg^{-1}) and stability (capacity retention: 88%) in half- and full-cell tests compared to the NCM (discharge capacity: 179 mAh g^{-1}, energy density: 337 Wh kg^{-1}, capacity retention: 63%).

Supplementary Materials: The following are available online at http://www.mdpi.com/1996-1073/13/18/4808/s1, Table S1: Comparison of d spacing and c lattice constant values of the samples. Figure S1: XPS survey spectra of (a) NCM and (b) NCMF. Figure S2: The 100th charge/discharge curves of NCM and NCMF at a current density of 100 mA g^{-1} in the potential range of 2.8–4.3 V vs. Li/Li^+ for 100 cycles. Figure S3: (a) Single titration profile of the sample during discharging in GITT. (b) Plots of discharge potential of the samples during three discharge cycles in the potential range 2.8–4.3 V vs. Li/Li^+. Table S2: Area ratios of oxygen (O) vacancies and metal–oxygen (M–O) bonds in NCM and NCMF.

Author Contributions: Conceptualization, H.K.; methodology, H.K.; formal analysis, H.K. and S.-B.K.; writing—original draft preparation, H.K.; data curation, D.-H.P.; supervision, K.-W.P.; project administration, K.-W.P.; writing—review and editing, K.-W.P. All authors have read and agreed to the published version of the manuscript.

Funding: This research was supported by the National Research Foundation (NRF) (2019M3E6A1104186 and 2020R1A2C2010510)).

Acknowledgments: This research was supported by the NRF.

Conflicts of Interest: The authors declare no conflict of interest.

References

1. Schipper, F.; Nayak, P.K.; Erickson, E.M.; Amalraj, S.F.; Srur-Lavi, O.; Penki, T.R.; Talianker, M.; Grinblat, J.; Sclar, H.; Breuer, O.; et al. Study of Cathode Materials for Lithium-Ion Batteries: Recent Progress and New Challenges. *Inorganics* **2017**, *5*, 32. [CrossRef]
2. Xia, Y.; Zheng, J.; Wang, C.; Gu, M. Designing principle for Ni-rich cathode materials with high energy density for practical applications. *Nano Energy* **2018**, *49*, 434–452. [CrossRef]
3. Ali, M.U.; Zafar, A.; Nengroo, S.H.; Hussain, S.; Alvi, M.J.; Kim, H.-J. Towards a Smarter Battery Management System for Electric Vehicle Applications: A Critical Review of Lithium-Ion Battery State of Charge Estimation. *Energies* **2019**, *12*, 446. [CrossRef]
4. Liu, L.; Li, M.; Chu, L.; Jiang, B.; Ruoxu, L.; Xiaopei, Z.; Cao, G. Layered ternary metal oxides: Performance degradation mechanisms as cathodes, and design strategies for high-performance batteries. *Prog. Mater. Sci.* **2020**, *111*, 100655. [CrossRef]
5. Manthiram, A. A reflection on lithium-ion battery cathode chemistry. *Nature Comm.* **2020**, *11*, 1550. [CrossRef]
6. Kwon, J.-S.; Lee, S.-E.; Lim, J.-H.; Choi, J.; Kim, J. Performance and Life Degradation Characteristics Analysis of NCM LIB for BESS. *Electronics* **2018**, *7*, 406. [CrossRef]
7. Xu, L.; Zhou, F.; Liu, B.; Zhou, H.; Zhang, Q.; Kong, J.; Wang, Q. Progress in Preparation and Modification of $LiNi_{0.6}Mn_{0.2}Co_{0.2}O_2$ Cathode Material for High Energy Density Li-Ion Batteries. *Int. J. Electrochem.* **2018**. [CrossRef]
8. Sun, G.; Yin, X.; Yang, W.; Zhang, J.; Du, Q.; Ma, Z.; Shao, G.; Wang, Z.-B. Synergistic effects of ion doping and surface-modifying for lithium transition-metal oxide: Synthesis and characterization of La_2O_3-modified $LiNi_{1/3}Co_{1/3}Mn_{1/3}O_2$. *Electrochim. Acta* **2018**, *272*, 11–21. [CrossRef]
9. Park, S.; Kim, D.; Ku, H.; Jo, M.; Kim, S.; Song, J.; Yu, J.; Kwon, K. The effect of Fe as an impurity element for sustainable resynthesis of $Li[Ni_{1/3}Co_{1/3}Mn_{1/3}]O_2$ cathode material from spent lithium-ion batteries. *Electrochim. Acta* **2019**, *296*, 814–822. [CrossRef]
10. Liang, L.; Zhang, W.; Zhao, F.; Denis, D.K.; Zaman, F.U.; Hou, L.; Yuan, C. Surface/Interface Structure Degradation of Ni-Rich Layered Oxide Cathodes toward Lithium-Ion Batteries: Fundamental Mechanisms and Remedying Strategies. *Adv. Mater. Interfaces* **2020**, *7*, 1901749. [CrossRef]
11. Zhang, S.S. Problems and their origins of Ni-rich layered oxide cathode materials. *Energy Storage Mater.* **2020**, *24*, 247–254. [CrossRef]
12. Li, T.; Yuan, X.-Z.; Zhang, L.; Song, D.; Shi, K.; Bock, C. Degradation Mechanisms and Mitigation Strategies of Nickel-Rich, NMC-Based Lithium-Ion Batteries. *Electrochem. Energy Rev.* **2020**, *3*, 43–80. [CrossRef]
13. Li, G.; Qi, L.; Xiao, P.; Yu, Y.; Chen, X.; Yang, W. Effect of precursor structures on the electrochemical performance of Ni-rich $LiNi_{0.88}Co_{0.12}O_2$ cathode materials. *Electrochim. Acta* **2018**, *270*, 319–329. [CrossRef]
14. Schipper, F.; Dixit, M.; Kovacheva, D.; Talianker, M.; Haik, O.; Grinblat, J.; Erickson, E.M.; Ghanty, C.; Major, D.T.; Markovsky, B.; et al. Stabilizing nickel-rich layered cathode materials by a high-charge cation doping strategy: Zirconium-doped $LiNi_{0.6}Co_{0.2}Mn_{0.2}O_2$. *J. Mater. Chem. A* **2016**, *4*, 16073–16084. [CrossRef]
15. Xue, L.; Zhang, Q.; Zhu, X.; Gu, L.; Yue, J.; Xia, Q.; Xing, T.; Chen, T.; Yao, Y.; Xia, H. 3D $LiCoO_2$ nanosheets assembled nanorod arrays via confined dissolution-recrystallization for advanced aqueous lithium-ion batteries. *Nano Energy* **2019**, *56*, 463–472. [CrossRef]
16. Jang, B.-C.; Son, J.-T. Structural Characterization of New Composition Core–Shell $Li[(Ni_{0.88}Co_{0.07}Al_{0.05})x(Ni_{0.55}Co_{0.2}Mn_{0.2}Al_{0.05})y]O_2$ Spherical Particles as a Cathode Material for Lithium-Ion Batteries. *J. Nanosci. Nanotechnol.* **2016**, *16*, 10681. [CrossRef]
17. Do, S.J.; Santhoshkumar, P.; Kang, S.H.; Prasanna, K.; Jo, Y.N.; Lee, C.W. Al-Doped $Li[Ni_{0.78}Co_{0.1}Mn_{0.1}Al_{0.02}]O_2$ for High Performance of Lithium Ion Batteries. *Ceram. Int.* **2019**, *45*, 6972–6977. [CrossRef]
18. Breddemann, U.; Erickson, E.M.; Davis, V.; Schipper, F.; Ellwanger, M.; Daub, M.; Hoffmann, A.; Erk, C.; Markovsky, B.; Aurbach, D.; et al. Fluorination of Li-Rich Lithium-Ion-Battery Cathode Materials by Fluorine Gas: Chemistry, Characterization, and Electrochemical Performance in Half Cells. *ChemElectroChem* **2019**, *6*, 3337–3349. [CrossRef]
19. Wei, Z.; Zhao, D.; He, H.; Cao, W.; Dong, G. A noise-tolerant model parameterization method for lithium-ion battery management system. *Appl. Energy* **2020**, *268*, 114932. [CrossRef]

20. Wei, Z.; Zhao, J.; Ji, D.; Tseng, K.J. A multi-timescale estimator for battery state of charge and capacity dual estimation based on an online identified model. *Appl. Energy* **2017**, *204*, 1264–1274. [CrossRef]
21. Xiao, X.; Liu, X.; Qiao, L.; Li, S. A Li-ion Battery Management System Based on MCU and OZ8920. *Procedia Eng.* **2012**, *29*, 738–743. [CrossRef]
22. Kong, F.; Liang, C.; Longo, R.C.; Yeon, D.-H.; Zheng, Y.; Park, J.-H.; Doo, S.-G.; Cho, K. Conflicting Roles of Anion Doping on the Electrochemical Performance of Li-Ion Battery Cathode Materials. *Chem. Mater.* **2016**, *28*, 6942–6952. [CrossRef]
23. Binder, J.O.; Culver, S.P.; Pinedo, R.; Weber, D.A.; Friedrich, M.S.; Gries, K.I.; Volz, K.; Zeier, W.G.; Janek, J. Investigation of Fluorine and Nitrogen as Anionic Dopants in Nickel-Rich Cathode Materials for Lithium-Ion Batteries. *ACS Appl. Mater. Interfaces* **2018**, *10*, 44452–44462. [CrossRef] [PubMed]
24. Yue, P.; Wang, Z.; Guo, H.; Xiong, X.; Li, X. A low temperature fluorine substitution on the electrochemical performance of layered $LiNi_{0.8}Co_{0.1}Mn_{0.1}O_2$−zFz cathode materials. *Electrochim. Acta* **2013**, *92*, 1–8. [CrossRef]
25. Vanaphuti, P.; Chen, J.; Cao, J.; Bigham, K.; Chen, B.; Yang, L.; Chen, H.; Wang, Y. Enhanced Electrochemical Performance of the Lithium-Manganese-Rich Cathode for Li-Ion Batteries with Na and F CoDoping. *ACS Appl. Mater. Interfaces* **2019**, *11*, 37842–37849. [CrossRef] [PubMed]
26. Wang, Q.; Zhang, L.; Zhao, P.; Du, Z. Facile Synthesis of a High-Capacity $LiNi_{0.8}Co_{0.15}Al_{0.05}O_2$ Nanoplate Cathode with a {010} Orientation for Lithium-ion Batteries Naval Research. *Int. J. Electrochem. Sci.* **2018**, *13*, 10382–10389. [CrossRef]
27. Kim, J.-H.; Park, K.-J.; Kim, S.J.; Yoon, C.S.; Sun, Y.-K. A method of increasing the energy density of layered Ni-rich Li[Ni1-2xCoxMnx]O_2 cathodes(x = 0.05, 0.1, 0.2). *J. Mater. Chem. A* **2019**, *7*, 2694–2701. [CrossRef]
28. Park, K.-J.; Choi, M.-J.; Maglia, F.; Kim, S.-J.; Kim, K.-H.; Yoon, C.S.; Sun, Y.-K. High-Capacity Concentration Gradient $Li[Ni_{0.865}Co_{0.120}Al_{0.015}]O_2$ Cathode for Lithium-Ion Batteries. *Adv. Energy Mater.* **2018**, *8*, 1703612. [CrossRef]
29. Tang, W.; Chen, Z.; Xiong, F.; Chen, F.; Huang, C.; Gao, Q.; Wang, T.; Yang, Z.; Zhang, W. An effective etching-induced coating strategy to shield $LiNi_{0.8}Co_{0.1}Mn_{0.1}O_2$ electrode materials by $LiAlO_2$. *J. Power Sources* **2019**, *412*, 246–254. [CrossRef]
30. Li, H.; Zhou, P.; Liu, F.; Li, H.; Cheng, F.; Chen, J. Stabilizing nickel-rich layered oxide cathodes by magnesium doping for rechargeable lithium-ion batteries. *Chem. Sci.* **2019**, *10*, 1374. [CrossRef]
31. Chen, J.; Yang, H.; Li, T.; Liu, C.; Tong, H.; Chen, J.; Liu, Z.; Xia, L.; Chen, Z.; Duan, J.; et al. The Effects of Reversibility of H2-H3 Phase Transition on Ni-Rich Layered Oxide Cathode for High-Energy Lithium-Ion Batteries. *Front. Chem.* **2019**. [CrossRef] [PubMed]
32. Liu, Q.; Chen, Q.; Zhang, Q.; Xiao, Y.; Zhong, X.; Dong, G.; Delplancke-Ogletree, M.-P.; Terryn, H.; Baert, K.; Reniers, F.; et al. In situ electrochromic efficiency of a nickel oxide thin film: Origin of electrochemical process and electrochromic degradation. *J. Mater. Chem. C* **2018**, *6*, 646. [CrossRef]
33. Pei, C.; Gu, Y.; Liu, Z.; Yu, X.; Feng, L. Iron-nickel layered double hydroxide boosted by simple fluoridation with enhanced performance for electrochemical oxygen evolution reaction. *ChemSusChem* **2019**, *12*. [CrossRef] [PubMed]
34. Kumar, S.K.; Ghosh, S.; Ghosal, P.; Martha, S.K. Synergistic effect of 3D electrode architecture and fluorine doping of $Li_{1.2}Ni_{0.15}Mn_{0.55}Co_{0.1}O_2$ for high energy density lithium-ion batteries. *J. Power Sources* **2017**, *356*, 115–123. [CrossRef]
35. Kim, D.; Shiiba, H.; Zettsu, N.; Yamada, T.; Kimijima, T.; Sánchez-Santolino, G.; Ishikawa, R.; Ikuhara, Y.; Teshima, K. Full picture discovery for mixed-fluorine anion effects on high-voltage spinel lithium nickel manganese oxide cathodes. *NPG Asia Mater.* **2017**, *9*. [CrossRef]
36. Zhang, Z.; Chen, D.; Chang, C. Improved electrochemical performance of $LiNi_{0.8}Co_{0.1}Mn_{0.1}O_2$ cathode materials via incorporation of rubidium cations into the original Li sites. *RSC Adv.* **2017**, *7*, 51721. [CrossRef]
37. Schipper, F.; Bouzaglo, H.; Dixit, M.; Erickson, E.M.; Weigel, T.; Talianker, M.; Grinblat, J.; Burstein, L.; Schmidt, M.; Lampert, J.; et al. From Surface ZrO_2 Coating to Bulk Zr Doping by High Temperature Annealing of Nickel-Rich Lithiated Oxides and Their Enhanced Electrochemical Performance in Lithium Ion Batteries. *Adv. Energy Mater.* **2017**, *8*, 1701682. [CrossRef]
38. Subramaniyam, C.M.; Celio, H.; Shiva, K.; Gao, H.; Goodneough, J.B.; Liu, H.K.; Dou, S.X. Long stable cycling of fluorine-doped nickel-rich layered cathodes for lithium batteries. *Sustain. Energy Fuels* **2017**, *1*, 1292. [CrossRef]

39. Choi, S.; Kim, M.-C.; Moon, S.-H.; Kim, H.; Park, K.-W. F-doped $Li_{1.15}Ni_{0.275}Ru_{0.575}O_2$ cathode materials with long cycle life and improved rate performance. *Electrochim. Acta* **2019**, *326*, 135015. [CrossRef]
40. Kim, H.; Kim, M.-C.; Choi, S.; Moon, S.-H.; Kim, Y.-S.; Park, K.-W. Facile one-pot synthesis of Ge/TiO_2 nanocomposite structures with improved electrochemical performance. *Nanoscale* **2019**, *11*, 17415. [CrossRef]
41. Zhang, M.; Zhao, H.; Tan, M.; Liu, J.; Hu, Y.; Liu, S.; Shu, X.; Li, H.; Ran, Q.; Cai, J.; et al. Yttrium modified Ni-rich $LiNi_{0.8}Co_{0.1}Mn_{0.1}O_2$ with enhanced electrochemical performance as high energy density cathode material at 4.5 V high voltage. *J. Alloys Compd.* **2019**, *774*, 82–92. [CrossRef]
42. Yang, J.; Xia, Y. Suppressing the Phase Transition of the Layered Ni-Rich Oxide Cathode during High-Voltage Cycling by Introducing Low-Content Li_2MnO_3. *ACS Appl. Mater. Interfaces* **2016**, *8*, 1297–1308. [CrossRef] [PubMed]
43. Jung, R.; Metzger, M.; Maglia, F.; Stinner, C.; Gasteiger, H.A. Oxygen Release and Its Effect on the Cycling Stability of LiNixMnyCozO_2 (NMC) Cathode Materials for Li-Ion Batteries. *J. Electrochem. Soc.* **2017**, *164*, A1361–A1377. [CrossRef]